IOP Publishing Smart Materials and Structures
Smart Mater. Struct. **23** (2014) 065003 (11pp) doi:10.1088/0964-1726/23/6/065003

# Development of self-healing polymers via amine–epoxy chemistry: I. Properties of healing agent carriers and the modelling of a two-part self-healing system

**He Zhang and Jinglei Yang**

School of Mechanical and Aerospace Engineering, Nanyang Technological University, Singapore

E-mail: mjlyang@ntu.edu.sg

Received 23 December 2013, revised 6 March 2014
Accepted for publication 21 March 2014
Published 16 April 2014

**Abstract**

Two types of healing agent carriers (microcapsules containing epoxy solution, referred to as EP-capsules, and etched hollow glass bubbles (HGBs) loaded with amine solution, referred to as AM-HGBs) used in self-healing epoxy systems were prepared and characterized in this study. The core percentages were measured at about 80 wt% and 33 wt% for EP-capsules and AM-HGBs, respectively. The loaded amine in AM-HGB, after incorporation into the epoxy matrix, showed high stability at ambient temperature, but diffused out gradually during heat treatment at 80 °C. The amount and the mass ratio of the two released healants at the crack plane were correlated with the size, concentration, and core percentage of the healing agent carriers. A simplified cubic array model for randomly distributed healing agent carriers was adopted to depict the longest diffusion distance of the released healants, which is inversely proportional to the cubic root of the carrier concentration.

Keywords: self-healing polymer, healing agent carriers, microcapsule, hollow glass bubble, modelling

(Some figures may appear in colour only in the online journal)

## 1. Introduction

The purpose of automatic self-healing is to enable materials to recover their original integrity and functions upon damage, without human intervention, by structural or molecular design [1]. The self-healing concept was first proposed in 1979 by Jud *et al* [2, 3] through molecular interdiffusion and was advanced by White *et al* [4] by embedding microcapsules containing healing liquid and catalyst particles into matrix material. In the latter approach, the epoxy matrix can automatically repair the cracks whenever and wherever they occur, to restore the mechanical properties of the epoxy matrix. In recent years this concept has been developed by many researchers, from both academia and industry, using various methods [5, 6], including the incorporation of microcapsules [7–20], embedment of hollow tubes [21–26] and microvascular networks [27–29], molecular interdiffusion [30, 31], as well as molecular design [32–40].

Although good healing performance was achieved in the first generation self-healing epoxy by the incorporation of dicyclopentadiene (DCPD)/Grubbs' catalyst, high cost due to the expensive Grubbs' catalyst and the instability of the Grubbs' catalyst in the hostile environment, limit its applications [4]. As epoxy resin is one of the most important matrices for structural composites, the exploration of self-healing based on epoxy chemistry is attracting more and more attention, with the aims being to maximize the material compatibility and minimize the cost. Currently, homogeneous

 

self-healing epoxy can be achieved by the above-mentioned approaches [11, 12, 23, 41–53], among which the incorporation of microcapsules containing healants is heavily investigated in the field because of the ease of manufacturing and material integrity.

Various epoxy monomers have been easily encapsulated using several methods [42, 54] due to their good emulsivity in an aqueous environment. However, the incorporation of suitable hardeners is rather challenging. The mechanism for the first embodiment of self-healing based on epoxy chemistry [42] is very similar to that of the DCPD/catalyst system [4]. The released epoxy monomers from poly(ureafomaldehyde) (PUF) microcapsules were cured or catalyzed by the dissociated reactive part from the pre-dispersed latent curing agent in the epoxy matrix upon heating. Since a high temperature of up to 130 °C is necessary for the dissociation and diffusion of the reactive part, this system is not a fully autonomous self-healing system. Considering the rapid curing rate of epoxy by polythiol at room temperature or even low temperature, Yuan *et al* [12, 44, 55]. encapsulated a polythiol using the *in situ* polymerization of a poly(melamineformaldehyde) (PMF) prepolymer. Good healing performance was observed both in the pure epoxy and carbon fiber/epoxy composite. Thinking of the high instability of the cationic catalyst, boron trifluoride diethyl etherate ($(C_2H_5)_2O \bullet BF_3$), in water and other media, Xiao *et al* [56]. explored a two-step method by first synthesizing hollow microcapsules using UV-initiated polymerization followed by infiltrating them with the catalyst. Adopting the curing chemistry by the cationic catalyst, they also used a plant's hollow sisal fibres to carry it for self-healing purpose [43]. High healing performance was achieved at room temperature when they incorporated the epoxy filled microcapsules and cationic loaded carriers into the epoxy matrix.

The above-mentioned curing agents are less frequently adopted hardeners for epoxy in practical applications. As for the widely used curing agents, i.e., polyamines or amine derivatives, the incorporation of them for self-healing purpose progresses at a slow pace. McIlroy *et al* [57] encapsulated a highly reactive amine derivative through the interfacial polymerization of isocyanate and amine in an inverse water-in-oil emulsion, but did not provide self-healing performance. Li *et al* [58] also encapsulated a polyetheramine by a solvent evaporation technique using poly(methylmethacrylate) (PMMA) as the shell material. Good healing performance was found at room temperature when epoxy matrix with excess reactive residual epoxide groups was incorporated with 15 wt% polyetheramine loaded microcapsules. Via a two-step method, Jin *et al* [45, 46] first synthesized hollow PUF polymeric microcapsules and then infiltrated them with commercialized amine hardeners, developing self-healing epoxy systems based on the encapsulated epoxy monomer and amine hardener using the two-part epoxy-amine chemistry. Excellent healing performance was obtained at room temperature. However, the long-term stability and the thermal stability of the polymeric shell of the microcapsules are strongly influenced by the corrosive amine [45]. How to fabricate mechanically robust and chemically stable healing agent carriers for reactive healants is a challenging topic in this area.

Our previous work [59] reported the fabrication of microcontainers through etching HGBs with diluted hydrofluoric acid (HF) solution in a specially designed mixer for self-healing applications. This study, as part I, mainly focuses on the systematical characterization of the two fabricated healing agent carriers and the modelling of a two-part self-healing system. The thermal stability of the amine solution in the HGBs was investigated after their embedment into the epoxy matrix. The model built by Rule *et al* [60] to address the available amount of healant on the fracture plane for one-part self-healing systems was adopted and further developed for a dual-capsule system in consideration of the stoichiometric match of two-part healants. In addition, a new model was explored to roughly deduce the longest diffusion distance of the released healant for mixing. The systematical investigation of the self-healing performance of this material system will be reported in part II.

## 2. Experiment

### 2.1. Materials

Epolam 5015 and hardener 5015 (Axson) were used as the epoxy matrix. Urea, formaldehyde, resorcinol, ammonium chloride ($NH_4Cl$), sodium hydroxide (NaOH), 1-octanol, diluted 1 wt% HF solution from concentrated form as etching agent, diethylenetriamine (DETA), 2,4,6-tris(dimethylaminomethyl)phenol (DMP 30) as the epoxy curing accelerator, ethyl phenyl acetate (EPA) as diluents for the epoxy, and acid yellow 73 as fluorescence, were purchased from Sigma-Aldrich (Singapore). The surfactant, ethylene maleic anhydride copolymer (EMA), was purchased from MP Biomedicals. The HGBs were ordered from 3M. All the chemicals were used as received unless otherwise specified.

### 2.2. Microencapsulation of the epoxy solution

The epoxy solution, 80 wt% Epolam 5015 in EPA, was encapsulated by the *in situ* polymerization of urea and formaldehyde in an oil-in-water emulsion at 350 rpm, which was specified in our previous report [59]. After collection, the microcapsules were sieved and collected in two ranges, 90–180 $\mu$m and 180–300 $\mu$m, as the small and large microcapsules. The pure shell material, PUF, was synthesized using the same procedure apart from the addition of core materials, epoxy solution. It was dried at room temperature (RT, ~20 °C) for 24 h before thermogravimetric analysis (TGA) testing.

### 2.3. Composition measurement for EP-capsules

Since the ranges of decomposition temperature for the shell material, PUF, and the core material, epoxy, overlap with each other [45, 61], it is impossible to use TGA to measure the composition for the EP-capsules. A physical separation method was proposed to assess the composition. First, a certain number of microcapsules were completely broken in a 20 ml vial using a Teflon rod. Later, the vial was charged with

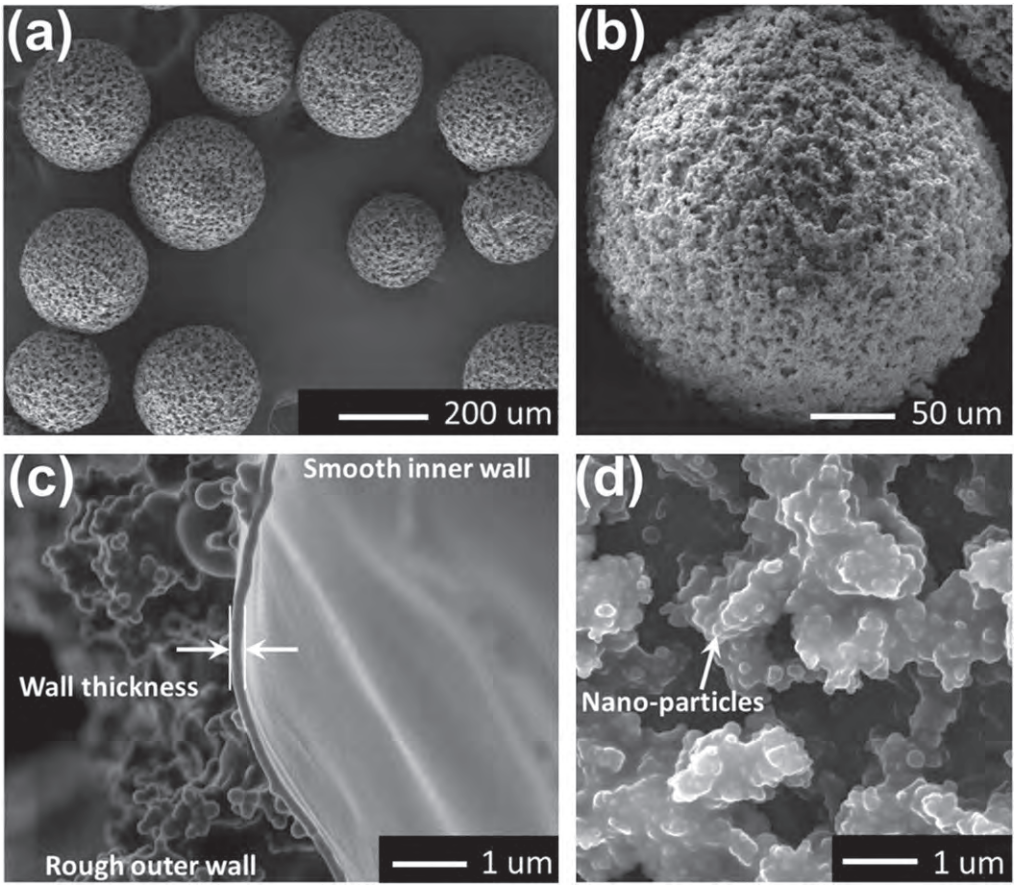


**Figure 1.** Overview (a), enlarged (b), cross-section (c), and the outer surface (d) of the synthesized EP-capsules of size $255.7 \pm 39.4\ \mu$m.

about 15 ml solvent, EPA, and then was shaken dramatically to wash the epoxy away from the shell. After that the mixture was separated using a Buchner funnel and rinsed with EPA three or four times to totally remove the residual epoxy. The filter paper with debris was further dried in an oven (Binder, Model V53) at 80 °C for 24 h to evaporate the solvent absorbed in the filter paper. Finally, the weight difference for the filter paper before and after separation was adopted to calculate the weight of the shell for the microcapsules used. To obtain an average core percentage of the microcapsules, five batches of microcapsules, of similar weight, were treated in the same way.

### *2.4. Preparation of AM-HGBs*

The procedures and devices used to etch HGBs and to fill the etched HGBs using a vacuum-assisted method were reported in our previous work [59]. In this study, well etched HGBs in two size ranges (38–63 $\mu$m and 63–90 $\mu$m) were adopted. Amine solution of DETA with DMP 30 at a ratio of 9:1 was infiltrated into the etched HGBs using the vacuum-assisted device as the curing agent. To visibly display and observe the thermal stability of the loaded amine in the HGBs, 0.5 wt% fluorescence, acid yellow 73, was mixed into the amine solution before the loading process.

### *2.5. Characterization methods*

The morphology, size, and shell thickness of the healing agent carriers were obtained from the field emission scanning electronic microscopy (FESEM) (JOEL JSM-7600F). Their size distributions of both the HGBs and microcapsules were measured from the SEM images using software, ImageJ, based on at least 100 pieces. The core content and the thermal stability of the healing agent carriers were characterized by TGA (AutoTGA 2950HR). In all the TGA tests, 10–30 mg powder samples were placed in a platinum pan and heated under a nitrogen atmosphere with a ramp rate of 10 °C $\text{min}^{-1}$. The dispersed healing agent carriers in the host matrix and their stability were assessed by optical microscopy (Olympus CKX41) with the fluorescent mode.

## 3. Results and discussion

### *3.1. Characterization of EP-capsules*

After sieving, the EP-capsules yield average diameters of $155.9 \pm 23.7\ \mu$m and $255.7 \pm 39.4\ \mu$m for the intervals 90–180 $\mu$m and 180–300 $\mu$m, respectively. Figure 1(a) shows the SEM image of the synthesized large microcapsules ($255.7 \pm 39.4\ \mu$m). Similar to reports in [8, 62], the wall of the microcapsules consist of outer rough porous shell

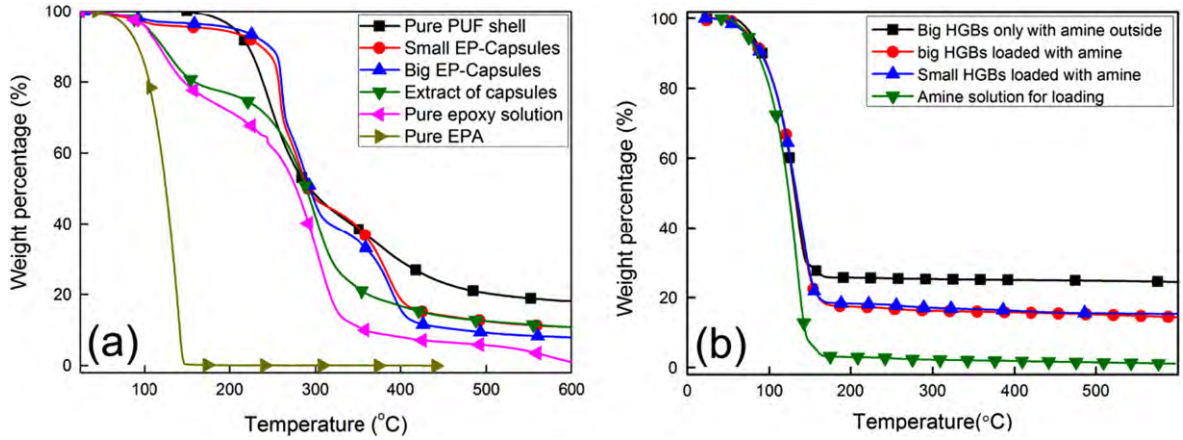


**Figure 2.** (a) TGA curves of the pure PUF shell, small microcapsules, large microcapsules, extract from the capsules, pure core solution and pure EPA; (b) TGA curves of the amine loaded small HGB, amine loaded large HGB, large HGB only absorbing amine solution outside, and pure amine solution.

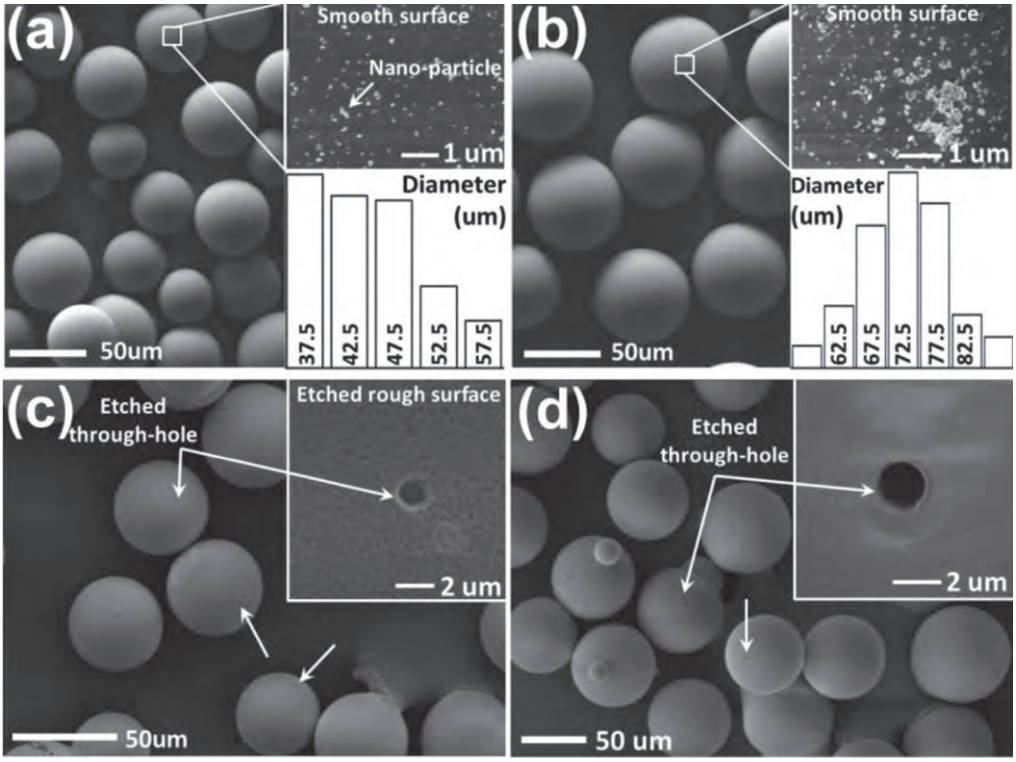


**Figure 3.** SEM images of (a) the original small HGBs, (b) original large HGBs, (c) etched small HGBs, and (d) etched large HGBs. The inserts in the top right show the outer surface of the original and etched HGBs, and the insets in the bottom right show the size distribution of the adopted HGBs.

(figures 1(b) and (d)) and inner smooth dense membrane (figure 1(c)) with a thickness of $165 \pm 17$ nm, which is quite uniform and very similar to that in [8, 62]. As in [62], the deposited PUF nano-particles almost surround all of the outer surface of the microcapsules (figures 1(a) and (b)), which provides the microcapsules with good protection from being broken accidentally and stronger interfacial strength with the host matrix when they are incorporated into host matrices.

Figure 2(a) shows the TGA curves of the small and large microcapsules, the pure shell material (PUF), the extract from the microcapsules, the pure core material for encapsulation, as well as pure EPA, respectively. Firstly, it could be concluded that the compositions of the microcapsules of two neighboring sizes are very similar to each other, which was demonstrated by the coincidence of the two TGA curves for the two adopted capsule sizes. Secondly, it is observed that the decomposition temperatures for PUF and epoxy resin overlap with each other [45, 61]. As a consequence of this, we are unable to use the TGA curve to calculate the composition of this microcapsule. Another method was employed to estimate the ratio of core to

shell for the microcapsules, as described in the experimental section. Using that method, the measured core percentage ($\omega_E$) was found to be about 79.7 ± 3.5 wt%, which is pretty close to that of the microcapsule containing epoxy resin obtained by Yuan *et al* [61] but a little lower than the core content of the PUF microcapsule with DCPD [8]. Thirdly, the core material of the microcapsules was extracted by squeezing the microcapsules in a syringe and collecting the liquid at the needle tip. It can be seen that the composition of the core material does not change during the encapsulation process by comparing the two TGA curves of the pure epoxy solution and the extracted core material from the microcapsules. This observation is consistent with the result by Blaiszik *et al* [62] when they fabricated microcapsules containing low concentration epoxy solution. Considering the core percentage of the microcapsules (about 80 wt%) and the composition of the core material (80 wt% epoxy in EPA), the weight percentage of epoxy in the microcapsules is about 64 wt% and the percentage of the solvent EPA should be about 16 wt%. Fourthly, by checking the TGA curves of pure EPA, epoxy solution, and the extract from the microcapsules, pure EPA evaporates completely before about 150 °C. However, the weight loss for both the small and large microcapsules detected before 150 °C is only about 3–4 wt%. This small weight loss is attributed to the trace water and diffused EPA on the microcapsule shell. This result indicates that the core material is well protected by the dense inner wall of the microcapsules. With the increase of the heating temperature up to 250 °C, the PUF shell is gradually decomposed and the core material rapidly evaporates or is decomposed, leading to the sharp drop in the weight in the TGA curves at around 250 °C.

### 3.2. Characterization of AM-HGBs

Figures 3(a) and (b) illustrate the original small and large HGBs adopted in this investigation, and the insets at the top right show the enlarged sites of the chosen bubbles. Before being etched, the outer shell of both the small and large HGBs are dotted with glass nano-particles. The insets at the bottom right of figures 3(a) and (b) describe the size distribution of the adopted HGBs. The measured diameters of the small and large HGBs are 45.1 ± 7.5 $\mu$m and 67.4 ± 7.4 $\mu$m, respectively. Figures 3(c) and (d) illustrate the etched small and large HGBs after water-deposition to remove the debris. After the etching process, small through-holes at micron level form and the uniformly distributed etching pits replace the attached glass nano-particles, as shown in the insets in figures 3(c) and (d). The measured diameters are 44.9 ± 6.2 $\mu$m and 66.9 ± 8.2 $\mu$m for the etched bubbles in 38–63 $\mu$m and 63–90 $\mu$m, respectively. The shell thickness changes from 1.16 ± 0.57 $\mu$m for the original HGBs to 0.79 ± 0.41 $\mu$m for the etched HGBs. The large variation in shell thicknesses for the etched HGBs means that a number of them have a relatively thicker shell, which will significantly influence their rupturability on the fracture surface upon the fracture event, when they are incorporated into a polymeric host as healing agent carriers.

Figure 3(b) shows the TGA curves for both small and large HGBs loading with amine using the vacuum-assisted device and HGBs just absorbing amine outside the shell. The coincidence of the two TGA curves for the small and large HGBs indicates that the neighboring sizes have no effect on the composition of the AM-HGBs, which is identical to that of the EP-capsules. The amine solution carried inside the HGBs is the most important parameter for the AM-HGBs. In order to simplify the description of how to obtain it, a new parameter, $\lambda$, defined by the mass ratio of the loaded amine to the shell of the etched HGB, is introduced here. It is easy to find that the mass ratio of the residual amine absorbed outside to the shell of the HGB ($\lambda_{out}$) is about 3, based on the TGA of HGBs with only amine outside. In addition, from the TGA curve for the HGBs loaded by the vacuum-assisted method, the mass ratio of the amine in total, including both amine inside and outside, to the shell ($\lambda_{total}$) is about 5. Consequently, the mass ratio of amine inside to the shell ($\lambda_{in}$) is 2. And finally, the percentage of the amine inside the shell ($\omega_A$) of about 33 wt% could be obtained by the following equation:

$$\omega_A = \frac{\lambda_{in}}{1 + \lambda_{in} + \lambda_{out}} \tag{1}$$

The range of the core percentage for the deposited HGBs during the loading process could also be achieved by theoretical calculation. Its lower limit is determined by the requirement for the deposition of the loaded HGB in the amine solution, that is, the density of the loaded etched HGB should be larger than the density of the amine solution, as indicated below by:

$$\frac{(\lambda_{min} + 1)4\pi\left(\frac{d_0}{2}\right)^2 t\rho_{HGB}}{\frac{4}{3}\pi\left(\frac{d_0}{2}\right)^3} = \rho_{amine} \tag{2}$$

where $\lambda_{min}$ is the minimum mass ratio of the amine inside to the glass shell, $d_0$ is the diameter of the outer shell (66.9 ± 8.2 $\mu$m), $t$ is the shell thickness of the etched HGB (0.79 ± 0.41 $\mu$m), $\rho_{HGB}$ and $\rho_{amine}$ are the density of the glass (2.55 g cm$^{-3}$ by the supplier) and the amine solution (0.95 g cm$^{-3}$), respectively. The calculated $\lambda_{min}$ when all the specific values are substituted in is:

$$\lambda_{min} = 4.25 \tag{3}$$

The upper limit is controlled by the cavity inside the shell to carry the amine solution. The highest core percentage occurs when the whole cavity of the HGB is taken up by the amine solution, as explained by the following equation:

$$\lambda_{max} = \frac{\rho_{amine}\frac{4}{3}\pi\left(\frac{d_0}{2}\right)^3}{\rho_{HGB}4\pi\left(\frac{d_0}{2}\right)^2 t} = \frac{\rho_{amine}}{\rho_{HGB}}\frac{d_0}{6t} \tag{4}$$

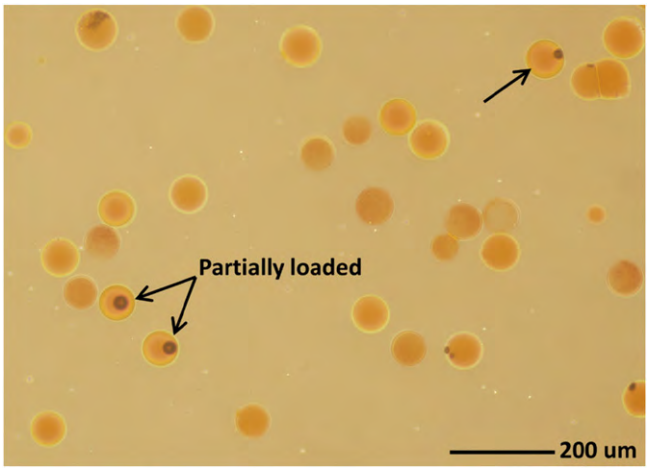


**Figure 4.** Epoxy thin film dispersed with 5 wt% AM-HGBs immediately after their incorporation.

After substitution, the calculated $\lambda_{max}$ is:

$$\lambda_{max} = 5.25 \tag{5}$$

Given the fact that there is residual amine solution outside the shell, the lower limit $\left(\omega_A^{min}\right)$ and the upper limit $\left(\omega_A^{max}\right)$ of the percentage for the loaded amine can be expressed as follows:

$$\omega_A^{min} = \frac{\lambda_{min}}{1 + \lambda_{min} + \lambda_{out}} = 51.5\% \tag{6}$$

$$\omega_A^{max} = \frac{\lambda_{max}}{1 + \lambda_{max} + \lambda_{out}} = 56.8\% \tag{7}$$

It is evident that the experimental measurement, 33 w%, seriously deviates from this theoretically derived range for the core percentage. Two reasons should account for this deviation. Firstly, some amine inside can be extracted out during the separation process when tissue is used to absorb the residual amine outside. Secondly, not all the empty or partially loaded HGBs can be separated completely during the separation process using this kind of method. These two factors would reduce the core percentage to some extent. Figure 4 shows the epoxy thin film dispersed with 5 wt% AM-HGBs right after their incorporation. Although most of the HGBs are fully loaded with amine solution, there are still some of them which are just partially loaded, as indicated by the arrows in the figure.

From the theoretical calculation, the two values, $\lambda_{min}$ and $\lambda_{max}$, are pretty close to each other, which means most of the cavity of the bubble is taken by amine after its deposition. The minimum occupied cavity ($v_{min}$) can be expressed by the following equation:

$$v_{min} = \frac{\frac{\lambda_{min} m_{Shell}}{\rho_{amine}}}{\frac{4}{3}\pi\left(\frac{d_1}{2}\right)^3} = \frac{\lambda_{min}}{\lambda_{max}} \tag{8}$$

The minimum occupied percentage, as high as 81%, is found when the loaded HGBs begin to deposit during the loading process.

### 3.3. Thermal stability of AM-HGBs

The thermal stability of the chemicals loaded in HGBs, and the HGBs themselves, is of great significance for practical applications since exothermal reactions and heat treatment are common in polymeric materials. Amine solution stained with 0.5 wt% yellow acid 73 was selected as the targeting core material for color indication and fluorescence after it was infiltrated into the etched HGBs.

To evaluate the thermal stability of the loaded amine in the HGBs in the target matrix, epoxy thin film dispersed with EP-capsules and AM-HGBs was prepared between two glass slides for optical observation. Figure 5 shows the dispersion of EP-capsules (large spheres) and AM-HGBs (small spheres) with a total concentration of 10 wt% and ratio of 1:3 for EP-capsule to AM-HGB in the epoxy film after different heat treatments. Arrow 1 in (a) and (b), arrow 2 in (c) and (d), and arrow 3 in (e) and (f), indicate the same HGB in the fully loaded, partially loaded, and empty conditions, respectively, after the heat treatments as shown at the bottom right of the corresponding graphs. Figures 5(a) and (b) give the optical images of the epoxy film after the epoxy was cured at RT for 24 h. The HGBs fully loaded with amine are yellow transparent dots under optical mode (arrow 1 in figure 5(a)) and bright green dots under fluorescent mode (arrow 1 in figure 5(b)) due to the added fluorescence. Although almost all the HGBs were fully infiltrated with amine solution as shown in figure 5(a), some fluorescent tails can be seen under the fluorescent mode (figure 5(b)), which means some of the amine escapes during the sample preparation. Figures 5(c) and (d) illustrate the epoxy film after being further cured at 35 °C for 24 h from the same site as figures 5(a) and (b). It is observed that some of the AM-HGBs partially lost their amine from inside, as indicated by the arrows. After further heat-treatment at 80 °C for 16 h, some of the AM-HGBs fully lost their amine from inside, turning to black dots under optical mode and annular eclipses under fluorescent mode, as indicated by arrow 3 in both figures 5(e) and (f). Figure 6 describes the quantitative assessment of the AM-HGBs in terms of the number percentage of HGBs which are loaded (e.g. arrow 1 in figures 5(a) and (b) and arrow 2 in figures 5(c) and (d)) and empty (e.g. arrow 3 in figures 5(e) and (f)) with amine as functions of the curing and heat treatment history. More than 400 individuals of each status were taken into account in the measurements. The amine inside the shell showed high thermal stability at the curing stage when the epoxy sample was cured at RT for 24 h followed by 35 °C for another 24 h. Only about 2% of the HGBs completely lost their amine in the cavity. However, the amine solution was not so stable when the sample was post-treated at 80 °C for a certain duration. The percentage of the loaded HGBs fell dramatically during the first 8 h at 80 °C and then leveled off at about 80%. Those changes are reasonable considering the slow diffusion of the loaded amine through the etched small holes at RT and especially at elevated temperature. Nevertheless, the AM-HGBs show relatively high thermal stability. The major

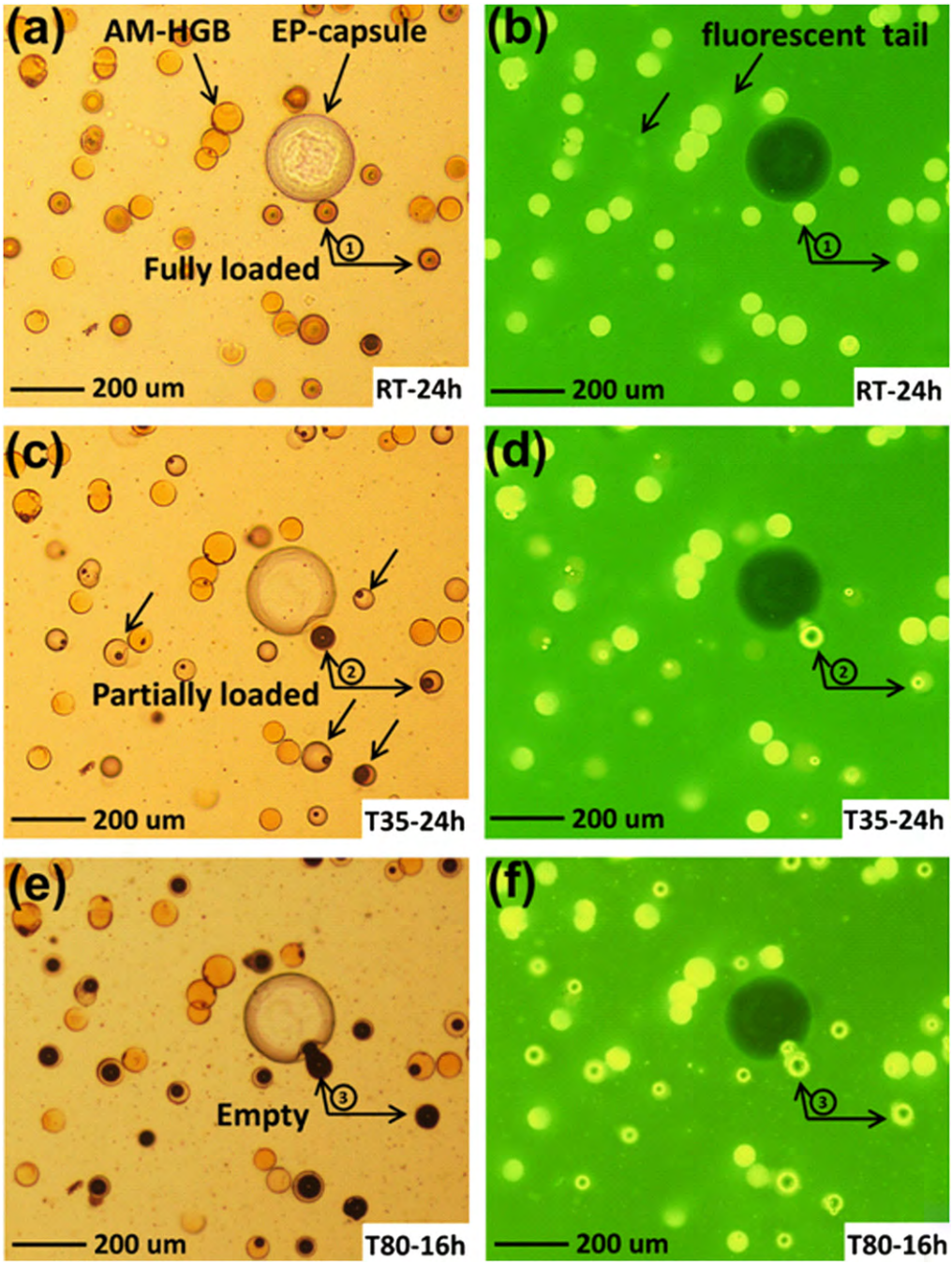


**Figure 5.** Optical microscopic images of the epoxy matrix with AM-HGBs (small spheres) and EP-capsules (large spheres) under both visible light mode (a, c, and e) and fluorescent mode (b, d, and f) after different heat treatments including: RT curing for 4 h (a and b), followed by curing at 35 °C for 24 h (c and d), and post treatment at 80 °C for 16 h (e and f). Arrow 1 in (a) and (b), 2 in (c) and (d), and 3 in (e) and (f) indicate the gradual loss of amine for one HGB during the heat treatments.

reason for this is that the small through-holes at micron level in the etched HGBs can be tightly sealed by the surroundings to retard or even impede the diffusion of the amine solution. Other factors which also contribute to the stability of the loaded amine include the dense structure, the chemical inertness, and the thermal stability of the glass shell after etching and heat-treatments. During the whole treatment, the HGBs remained the same as their original appearance in the field, demonstrating their highly thermal resistance and anti-corrosive performance as micro-containers.

### *3.4. Modelling of a dual-capsule self-healing system*

*3.4.1. Delivered healing agents on the fracture plane.* Rule *et al* [60] established the relationship for the areal density of the delivered healant $(\overline{m})$ with respect to the capsule size and concentration for a one-part self-healing system as follows:

$$\overline{m} = \frac{m_{\mathrm{h}}}{D} = \frac{nm_{\mathrm{c}}}{D} \tag{9}$$

where $m_{\mathrm{h}}$ means the total healing agent released at the fracture plane, $n$ means the number of microcapsules ruptured during

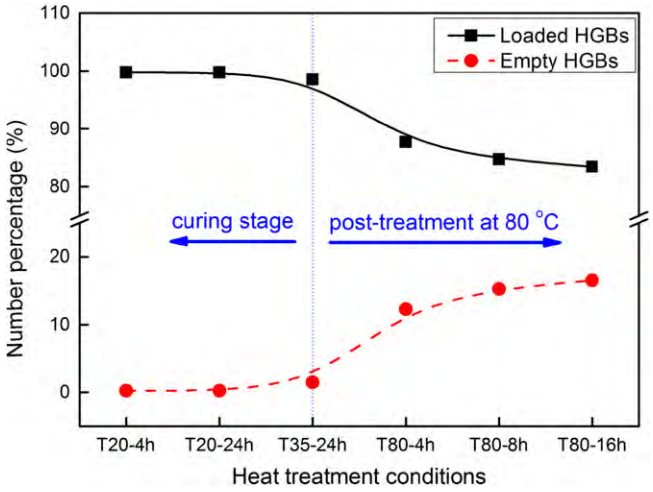


**Figure 6.** Number percentage of HGBs which are loaded (e.g. arrow 1 in figure 4(a) and arrow 2 in figure 4(b)) and empty (e.g. arrow 3 in figure 4(e)) with amine as a function of the curing and heat treatment history.

the fracture event, $m_c$ means the healing agent released by one single ruptured microcapsule, and $D$ means the crack area. This relationship assumes that all the randomly dispersed capsules intersected by the crack plane are ruptured and thereafter release the healing agent.

However, for this particular two-part self-healing system, three more factors, i.e. the size difference and core percentage difference of the two healing agent carriers, as well as the stoichiometric match of the two released healing agents, should be taken into consideration when such a relationship is to be established. As shown in figure 7, the two healing agent carriers, microcapsules (indicated by the large pink microspheres) and HGBs (indicated by the small yellow microspheres), are assumed to be randomly dispersed in the epoxy host. The crack plane, the grey zone with height $\overline{d_E}$ (the mean diameter of microcapsules) and the green zone with height $\overline{d_A}$ (the mean diameter of HGBs) are also shown in the scheme. As stated by Rule *et al* [60], the microcapsules with their center in the grey zone and the HGBs with their center in the green zone will be ruptured when the crack propagates along the crack plane. Considering the core percentage ($\omega_c$) of each healing agent carrier, the more precise $\overline{m}$ here should be:

$$\overline{m} = \frac{m_h}{D} = \frac{nm_c\omega_c}{D} \tag{10}$$

The number of healing agent carriers ($n$) ruptured at the crack plane was derived by Rule *et al* [60] as:

$$n = \frac{\rho_s D d_c \Phi_c}{m_c} \tag{11}$$

where $\rho_S$ is the sample density and $\Phi_c$ is the concentration of the healing agent carrier in the host.

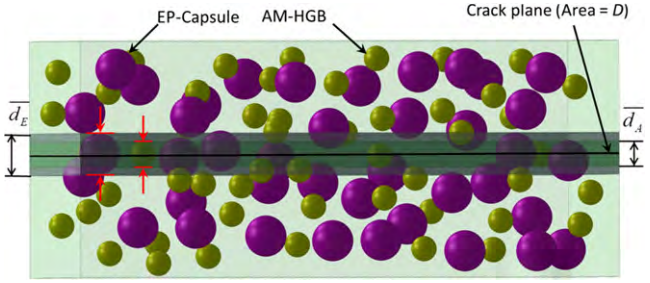


**Figure 7.** Scheme of capsules and HGBs randomly distributed in the epoxy matrix.

After the substitution of $n$ in equation (10), the final expression for $\overline{m}$ is:

$$\overline{m} = \rho_s d_c \Phi_c \omega_c \tag{12}$$

Considering the two-part feature, equation (12) is applicable to both the EP-capsules and the AM-HGBs. Consequently, the mass ratio of the two parts is:

$$\frac{\overline{m_E}}{\overline{m_A}} = \frac{\overline{d_E}}{\overline{d_A}} \cdot \frac{\Phi_E}{\Phi_A} \cdot \frac{\omega_E}{\omega_A} \tag{13}$$

where the subscripts, $E$ and $A$, mean the released epoxy and amine, respectively.

Equations (12) and (13) are the two governing equations for the healing performance of two-part self-healing systems. According to equation (12), the areal density of the released healing agent for each part is proportional to the density of the sample ($\rho_s$), the diameter of the healing agent carriers ($d_c$), the carrier concentration $\left(\Phi_c\right)$, and the core percentage of each single carrier ($\omega_c$). According to equation (13), the stoichiometry of the two healing agents $\left(\overline{m_E}/\overline{m_A}\right)$ is determined by the ratio of the mean diameters, the ratio of the concentrations, as well as the ratio of the core percentages for the two healing agent carriers.

*3.4.2. The longest diffusion distance of released healing agents.* The mixing of the released epoxy and hardener is of great significance in improving healing performance, considering the two-part stoichiometry. As the healing agent carriers locate at the fracture plane randomly and discretely, the longest diffusion distance from their carriers also plays an important role in this two-part system. Since the carriers were uniformly dispersed in the host matrix, a simple cubic array model of the randomly distributed carriers could be adopted to roughly calculate the longest distance with regard to the carrier concentration, as shown in figure 8. Each single carrier (microcapsule or HGB) is located at the center of a small cube with side length $a_0$. The number of simple cubes ($n$) is:

$$n = \frac{\Phi_c m_s}{m_c} \tag{14}$$

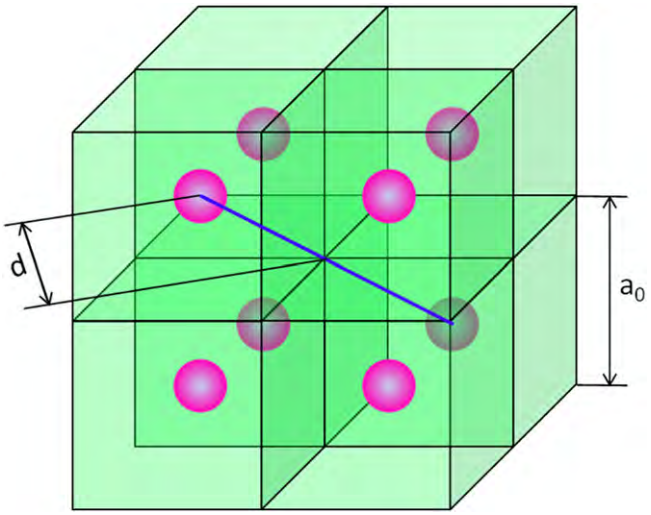


**Figure 8.** Proposed cubic distribution model to identify the maximum diffusion distance of the released healants from different healing agent carriers.

The total volume of the sample ($V_s$) and the volume of each single cube ($V_c$) can be expressed as:

$$V_s = \frac{m_s}{\rho_s} \tag{15}$$

$$V_c = \frac{V_s}{n} \tag{16}$$

Based on equations (14)–(16), the side length of the simple cube is:

$$a_0 = \sqrt[3]{\frac{m_c}{\rho_s \Phi}} \tag{17}$$

Finally, the longest diffusion distance is from the carrier to the cubic center:

$$d = \frac{\sqrt{3}}{2} a_0 = \frac{\sqrt{3}}{2} \cdot \sqrt[3]{\frac{m_c}{\rho_s \Phi}} \tag{18}$$

From equation (18), the longest diffusion distance is inversely proportional to the cube root of the carrier concentration, which is applicable to both the microcapsule and HGB. With a shorter diffusion distance at higher concentrations, better mixing and therefore better stoichiometry can be achieved, which might lead to improved healing performance.

## 4. Conclusions

In this study, EP-capsules and AM-HGBs were characterized. Models were established to address the available healants and the diffusion distance on the crack plane on the basis of two-part epoxy-amine stoichiometry. The following main conclusions can be drawn.

1. The core percentage for EP-capsules was found at 80 wt%, and for AM-HGBs it was at 33 wt%, which seriously deviates from the theoretical estimation of the amine in the etched HGBs.
2. Due to the cured epoxy matrix acting as a sealant outside the HGBs, the amine in the etched HGBs shows high thermal stability during the curing stage. However, some amine still leaks out through the shell during heat treatment at 80 °C.
3. The areal density of the delivered healant $(\overline{m})$ is proportional to the density of the sample, the diameter, concentration, and core percentage of the healing agent carriers, and the mass ratio of epoxy over amine $(\overline{m_E}/\overline{m_A})$ is determined by the ratio of the mean diameters, the ratio of the concentrations, and the ratio of the core percentages for the two healing agent carriers.
4. The longest diffusion distance of the released healing agent is inversely proportional to the cubic root of the concentration of the healing agent carrier, based on the simple cubic array model.

## Acknowledgement

Jinglei Yang greatly acknowledges the financial support of an NTU start-up grant and the Singapore Ministry of Education (Tier 1 grant no: RG17/09).

## References

[1] Yang J L, Zhang H and Huang M X 2012 Emerging technology in aerospace engineering: polymer based self-healing materials *Aerospace Materials Handbook* ed S Zhang and M Huang (Boca Raton, FL: CRC Press) pp 531–606
[2] Jud K and Kausch H H 1979 Load-transfer through chain molecules after interpenetration at interfaces *Polym. Bull.* **1** 697–707
[3] Jud K, Kausch H H and Williams J G 1981 Fracture-mechanics studies of crack healing and welding of polymers *J. Mater Sci.* **16** 204–10
[4] White S R, Sottos N R, Geubelle P H, Moore J S, Kessler M R, Sriram S R *et al* 2001 Autonomic healing of polymer composites *Nature* **409** 794–7
[5] Wu D Y, Meure S and Solomon D 2008 Self-healing polymeric materials: a review of recent developments *Prog. Polym. Sci.* **33** 479–522
[6] Jin H, Hart K R, Coppola A M, Gergely R C, Moore J S, Sottos N R *et al* 2013 Self-healing epoxies and their composites *Self-Healing Polymers* ed W H Binder (Weinheim: Wiley) pp 361–80
[7] Brown E N, Sottos N R and White S R 2002 Fracture testing of a self-healing polymer composite *Exp. Mech.* **42** 372–9
[8] Brown E N, Kessler M R, Sottos N R and White S R 2003 *In situ* poly(urea-formaldehyde) microencapsulation of dicyclopentadiene *J. Microencapsul.* **20** 719–30
[9] Cho S H, Andersson H M, White S R, Sottos N R and Braun P V 2006 Polydimethylsiloxane-based self-healing materials *Adv. Mater.* **18** 997–1000
[10] Yang J L, Keller M W, Moore J S, White S R and Sottos N R 2008 Microencapsulation of isocyanates for self-healing polymers *Macromolecules* **41** 9650–5

[11] Yin T, Zhou L, Rong M Z and Zhang M Q 2008 Self-healing woven glass fabric/epoxy composites with the healant consisting of micro-encapsulated epoxy and latent curing agent *Smart Mater. Struct.* **17** 015019
[12] Yuan Y C, Rong M Z and Zhang M Q 2008 Preparation and characterization of microencapsulated polythiol *Polymer* **49** 2531–41
[13] Huang M and Yang J 2011 Facile microencapsulation of HDI for self-healing anticorrosion coatings *J Mater. Chem.* **21** 11123–30
[14] Huang M, Zhang H and Yang J 2012 Synthesis of organic silane microcapsules for self-healing corrosion resistant polymer coatings *Corros. Sci.* **65** 561–6
[15] Kessler M R, Sottos N R and White S R 2003 Self-healing structural composite materials *Composites* A **34** 743–53
[16] Kessler M R and White S R 2001 Self-activated healing of delamination damage in woven composites *Composites* A **32** 683–99
[17] Beiermann B A, Keller M W and Sottos N R 2009 Self-healing flexible laminates for resealing of puncture damage *Smart Mater Struct.* **18** 085001
[18] Jin H, Miller G M, Pety S J, Griffin A S, Stradley D S, Roach D *et al* 2013 Fracture behavior of a self-healing, toughened epoxy adhesive *Int. J. Adhes. Adhes.* **44** 157–65
[19] Jin H, Miller G M, Sottos N R and White S R 2011 Fracture and fatigue response of a self-healing epoxy adhesive *Polymer* **52** 1628–34
[20] Moll J L, Jin H, Mangun C L, White S R and Sottos N R 2013 Self-sealing of mechanical damage in a fully cured structural composite *Compos. Sci. Technol.* **79** 15–20
[21] Dry C 1996 Procedures developed for self-repair of polymer matrix composite materials *Compos. Struct.* **35** 263–9
[22] Trask R S and Bond I P 2006 Biomimetic self-healing of advanced composite structures using hollow glass fibres *Smart Mater. Struct.* **15** 704–10
[23] Motuku M, Vaidya U K and Janowski G M 1999 Parametric studies on self-repairing approaches for resin infused composites subjected to low velocity impact *Smart Mater. Struct.* **8** 623–38
[24] Sinha-Ray S, Pelot D D, Zhou Z P, Rahman A, Wu X F and Yarin A L 2012 Encapsulation of self-healing materials by coelectrospinning, emulsion electrospinning, solution blowing and intercalation *J. Mater. Chem.* **22** 9138–46
[25] Wu X-F, Rahman A, Zhou Z, Pelot D D, Sinha-Ray S, Chen B *et al* 2013 Electrospinning core-shell nanofibers for interfacial toughening and self-healing of carbon-fiber/epoxy composites *J. Appl. Polym. Sci.* **129** 1383–93
[26] Wu X-F and Yarin A L 2013 Recent progress in interfacial toughening and damage self-healing of polymer composites based on electrospun and solution-blown nanofibers: An overview *J. Appl. Polym. Sci.* **130** 2225–37
[27] Therriault D, White S R and Lewis J A 2003 Chaotic mixing in three-dimensional microvascular networks fabricated by direct-write assembly *Nature Mater.* **2** 265–71
[28] Therriault D, Shepherd R F, White S R and Lewis J A 2005 Fugitive inks for direct-write assembly of three-dimensional microvascular networks *Adv. Mater.* **17** 395–9
[29] Williams H R, Trask R S and Bond I P 2007 Self-healing composite sandwich structures *Smart Mater. Struct.* **16** 1198–207
[30] Lin C B, Lee S B and Liu K S 1990 Methanol-induced crack healing in poly(methyl methacrylate) *Polym. Eng. Sci.* **30** 1399–406
[31] Caruso M M, Delafuente D A, Ho V, Sottos N R, Moore J S and White S R 2007 Solvent-promoted self-healing epoxy materials *Macromolecules* **40** 8830–2
[32] Chen X X, Dam M A, Ono K, Mal A, Shen H B, Nutt S R, Sheran K and Wudl F 2002 A thermally re-mendable cross-linked polymeric material *Science* **295** 1698–702
[33] Chung C M, Roh Y S, Cho S Y and Kim J G 2004 Crack healing in polymeric materials via photochemical 2 + 2 cycloaddition *Chem. Mat.* **16** 3982–4
[34] Burnworth M, Tang L M, Kumpfer J R, Duncan A J, Beyer F L, Fiore G L, Rowan S J and Weder C 2011 Optically healable supramolecular polymers *Nature* **472** 334–7
[35] Cordier P, Tournilhac F, Soulie-Ziakovic C and Leibler L 2008 Self-healing and thermoreversible rubber from supramolecular assembly *Nature* **451** 977–80
[36] Wang Q, Mynar J L, Yoshida M, Lee E, Lee M, Okuro K, Kinbara K and Aida T 2010 High-water-content mouldable hydrogels by mixing clay and a dendritic molecular binder *Nature* **463** 339–43
[37] Chen Y, Kushner A M, Williams G A and Guan Z 2012 Multiphase design of autonomic self-healing thermoplastic elastomers *Nature Chem.* **4** 467–72
[38] Ghosh B and Urban M W 2009 Self-Repairing Oxetane-Substituted Chitosan Polyurethane Networks *Science* **323** 1458–60
[39] Ramachandran D, Liu F and Urban M W 2012 Self-repairable copolymers that change color *RSC Adv.* **2** 135–43
[40] Du P F, Liu X X, Zheng Z, Wang X L, Joncheray T and Zhang Y F 2013 Synthesis and characterization of linear self-healing polyurethane based on thermally reversible Diels-Alder reaction *RSC Adv.* **3** 15475–82
[41] Caruso M M, Blaiszik B J, White S R, Sottos N R and Moore J S 2008 Full recovery of fracture toughness using a nontoxic solvent-based self-healing system *Adv. Funct. Mater.* **18** 1898–904
[42] Yin T, Rong M Z, Zhang M Q and Yang G C 2007 Self-healing epoxy composites—preparation and effect of the healant consisting of microencapsulated epoxy and latent curing agent *Compos. Sci Technol.* **67** 201–12
[43] Xiao D S, Yuan Y C, Rong M Z and Zhang M Q A 2009 Facile Strategy for Preparing Self-Healing Polymer Composites by Incorporation of Cationic Catalyst-Loaded Vegetable Fibers *Adv. Funct. Mater.* **19** 2289–96
[44] Yuan Y C, Rong M Z, Zhang M Q, Chen B, Yang G C and Li X M 2008 Self-healing polymeric materials using epoxy/mercaptan as the healant *Macromolecules* **41** 5197–202
[45] Jin H, Mangun C L, Stradley D S, Moore J S, Sottos N R and White S R 2012 Self-healing thermoset using encapsulated epoxy-amine healing chemistry *Polymer* **53** 581–7
[46] Jin H, Mangun C L, Griffin A S, Moore J S, Sottos N R and White S R 2013 Thermally stable autonomic healing in epoxy using a dual-microcapsule system *Adv. Mater.* **26** 282–7
[47] Bleay S M, Loader C B, Hawyes V J, Humberstone L and Curtis P T 2001 A smart repair system for polymer matrix composites *Composites* A **32** 1767–76
[48] Pang J W C and Bond I P 2005 'Bleeding composites'—damage detection and self-repair using a biomimetic approach *Composites* A **36** 183–8
[49] Toohey K S, Hansen C J, Lewis J A, White S R and Sottos N R 2009 Delivery of two-part self-healing chemistry via microvascular networks *Adv. Funct. Mater.* **19** 1399–405
[50] Hansen C J, Wu W, Toohey K S, Sottos N R, White S R and Lewis J A 2009 Self-healing materials with interpenetrating microvascular networks *Adv. Mater.* **21** 4143–7
[51] Tian Q, Yuan Y C, Rong M Z and Zhang M Q 2009 A thermally remendable epoxy resin *J. Mater. Chem.* **19** 1289–96
[52] Williams G, Trask R and Bond I 2007 A self-healing carbon fibre reinforced polymer for aerospace applications *Composites* A **38** 1525–32
[53] Williams G J, Bond I P and Trask R S 2009 Compression after impact assessment of self-healing CFRP *Composites* A **40** 1399–406

[54] Xiao D S, Rong M Z and Zhang M Q 2007 A novel method for preparing epoxy-containing microcapsules via UV irradiation-induced interfacial copolymerization in emulsions *Polymer.* **48** 4765–76

[55] Yuan Y C, Ye Y, Rong M Z, Chen H, Wu J, Zhang M Q, Qin S X and Yang G C 2011 Self-healing of low-velocity impact damage in glass fabric/epoxy composites using an epoxy–mercaptan healing agent *Smart Mater. Struct.* **20** 015024

[56] Xiao D S, Yuan Y C, Rong M Z and Zhang M Q 2009 Hollow polymeric microcapsules: Preparation, characterization and application in holding boron trifluoride diethyl etherate *Polymer* **50** 560–8

[57] McIlroy D A, Blaiszik B J, Caruso M M, White S R, Moore J S and Sottos N R 2010 Microencapsulation of a reactive liquid-phase amine for self-healing epoxy composites *Macromolecules* **43** 1855–9

[58] Li Q, Mishra A K, Kim N H, Kuila T, Lau K-T and Lee J H 2013 Effects of processing conditions of poly (methyl-methacrylate) encapsulated liquid curing agent on the properties of self-healing composites *Composites* B **49** 6–15

[59] Zhang H and Yang J 2013 Etched glass bubbles as robust micro-containers for self-healing materials *J Mater. Chem.* A **1** 12715–20

[60] Rule J D, Sottos N R and White S R 2007 Effect of microcapsule size on the performance of self-healing polymers *Polymer* **48** 3520–9

[61] Yuan L, Liang G Z, Xie J Q, Li L and Guo J 2006 Preparation and characterization of poly(urea-formaldehyde) microcapsules filled with epoxy resins *Polymer* **47** 5338–49

[62] Blaiszik B J, Caruso M M, McIlroy D A, Moore J S, White S R and Sottos N R 2009 Microcapsules filled with reactive solutions for self-healing materials *Polymer* **50** 990–7